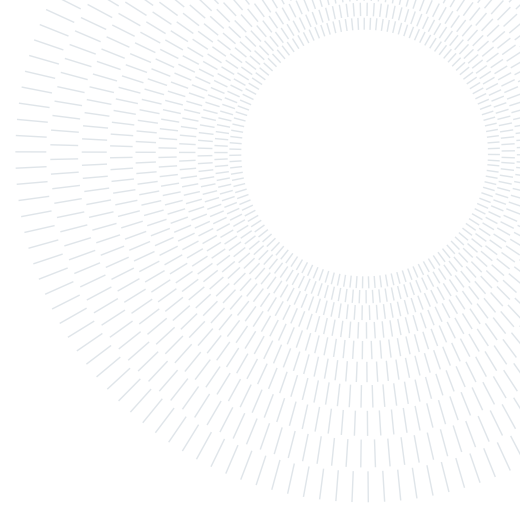**POLITECNICO**

MILANO 1863

SCUOLA DI INGEGNERIA INDUSTRIALE
E DELL'INFORMAZIONE

Parametric Study of Entry Vehicles with Hyperbolic Contours

Tesi di Laurea Magistrale in
Space Enginnering - Ingegneria Spaziale

Nemanja Janus, 10761243

Advisor:
Prof. Luigi Vigevano

Academic year:
2022-2023

Abstract: On all previous NASA missions to Mars, the shape of the front of the capsule reaching the planet's surface has been designed using a truncated cone with a spherical apex. An alternative shape of the capsule can be designed using hyperbolic contours. This work investigates the hypersonic aerodynamic characteristics of entry capsules on Mars, designed with hyperbolic contours, using the SU2-NEMO CFD code. The aerothermodynamic environment at one point in the entry phase is also analyzed. The results of the CFD simulations showed that the drag and lift coefficients can be increased using hyperbolic contours, compared to those of the original MSL entry vehicle, without significantly altering the shape of the capsule. This implies that the aerodynamic properties of the entry vehicle can be improved by using the front body shape based on hyperbolic contours.

Key-words: hypersonic flow, Mars entry vehicles, hyperbolic contours of the forebody

1. Introduction

Since the 1960s, a number of exploratory missions have been made to Mars. As the Mars landing probe enters the Martian atmosphere, it encounters non-air gas. Around the probe, there is hypersonic flow, which causes intense aerodynamic force and aero-heating on the probe surface. As a result, particular aerodynamic and thermal protection issues are raised. Earth reentry missions and Mars entry missions share certain parallels, but there is also a notable distinction. One of the recent Mars entry missions is called Mars Science Laboratory (MSL), which successfully landed on the Mars surface in August 2012. MSL's Entry, descent, and landing (EDL) system successfully delivered the 900-kg Curiosity rover to the surface of Mars [1]. One of the biggest obstacles in landing the probe onto Mars's surface is the thin atmosphere of Mars, which is approximately equal to 1 percent of the Earth's atmosphere. As a result, in order to decelerate the vehicle as much as possible, landing sites were chosen such that during descent, probes transverse as much atmosphere as possible. This resulted in landing sites several kilometers below the Martian "sea level". For this reason, MSL used guided entry with banking maneuvers to orient the lift vector to minimize range errors. The primary objective of adopting a guided lifting entry is to reach parachute deploy conditions (Mach number and dynamic pressure) at a high enough altitude to give the lander enough time to decelerate before touchdown. Because the interaction between the MSL aeroshell and the Martian atmosphere consumed more than 99 percent of the entry system's initial kinetic energy, largely in the form of heat, the MSL rover needed protection from aerothermodynamic stresses during hypersonic atmospheric entry. Because of this, MSL utilized a strong aeroshell and a lightweight ablator thermal protection system (TPS), both of which were identical to those utilized by earlier NASA missions to Mars [2]. The contour of the forebody of the capsule is designed based on the blunted nose cone. In particular, the forebody

shape is a 70-degree half-angle spherically blunted cone, which is also been used in previous NASA missions to Mars, starting form the Viking mission, but this time, the overall aeroshell dimensions were much higher. The large aeroshell and high ballistic coefficient, β_m, of MSL caused a boundary layer turbulent transition before peak heating, which was the first for a Mars entry heatshield and resulted in more extreme aerothermodynamic conditions [3]. Heat flux at the stagnation point increases proportionally to $\rho_\infty^{0.5} \cdot v_\infty^{3.15} \cdot R_N^{-0.5}$, where ρ_∞, v_∞, and R_N are the free stream density and velocity, and the blunt nose radius of the capsule, respectively. This relation suggests that for mitigating the heat flux, ρ_∞ and v_∞ should be reduced, and R_N should be large enough. For this reason, there is a need to reduce the ballistic coefficient, because when β_m is small, the capsule can be decelerated at a higher altitude compared to that with the higher β_m value [4]. As a result, both ρ_∞ and v_∞ can be reduced. This research will be focused on one of the possible ways to eliminate the problem of descending and landing on Mars's surface. In particular, in order to increase the deceleration of the vehicle at higher altitudes, the drag coefficient of the vehicle must be increased. Moreover, the increase in drag coefficient will be studied by means of modifying the shape of the forebody of the capsule itself. For this purpose, as a sample case, MSL capsule will be used. Instead of a combination of the arc and the inclined line, by using hyperbolic curves to design the forebody shape, the nose and cone area can be connected smoothly, and the nose bluntness and the half angle of the cone also can be modified easily. The aerothermodynamic environment is analyzed using 3D numerical simulations which are performed using SU2 NEMO CFD code, which provides the possibility to capture complex physics of high Mach number non-equilibrium multispecies flows.

The article is organized in the following way. First, a brief overview of the physical and numerical models implemented in the SU2-NEMO CFD code is presented in Section 2. In Section 3, two study cases for the non-equilibrium high Mach number flows are analyzed in order to validate SU2-NEMO capabilities. Furthermore, Section 4 presents a parametric study performed to investigate one possible way to improve descending and landing on Mars. That is, increasing the drag coefficient for the purpose of reducing the ballistic coefficient. Section 5 provides concluding remarks with suggestions for future work.

2. SU2 NEMO

SU2-NEMO is a computational fluid dynamics (CFD) code capable of simulating flows in thermo-chemical nonequilibrium, developed within the open-source multi-physics and optimization software, SU2 [5]. In this section, the governing equations, physical and numerical models implemented within the code as well as the most important boundary conditions are presented [6].

2.1. Physical Modeling

In the framework of SU2-NEMO, continuum hypersonic flows are modeled with the Navier–Stokes equations extended for reacting flows in thermochemical nonequilibrium. These equations are a set of coupled nonlinear partial differential equations, which can be seen below in Equation (1) [6].

$$\boldsymbol{R}(\boldsymbol{U}, \nabla \boldsymbol{U}) = \frac{\partial \boldsymbol{U}}{\partial t} + \nabla \cdot \boldsymbol{F}^c(\boldsymbol{U}) - \nabla \cdot \boldsymbol{F}^v(\boldsymbol{U}, \nabla \boldsymbol{U}) - \boldsymbol{Q}(\boldsymbol{U}) = \boldsymbol{0}, \tag{1}$$

where the conservative variables, convective flux, viscous flux, and source terms are given using standard notation for a number of species n_s by

$$\boldsymbol{U} = \left\{ \begin{array}{c} \rho_1 \\ \cdot \\ \cdot \\ \cdot \\ \rho_{n_s} \\ \rho\boldsymbol{u} \\ \rho e \\ \rho e^{ve} \end{array} \right\}, \boldsymbol{F}^c = \left\{ \begin{array}{c} \rho_1\boldsymbol{u} \\ \cdot \\ \cdot \\ \cdot \\ \rho_{n_s}\boldsymbol{u} \\ \rho\boldsymbol{u}\boldsymbol{u}^T + PI \\ \rho h\boldsymbol{u} \\ \rho e^{ve}\boldsymbol{u} \end{array} \right\}, \boldsymbol{F}^v = \left\{ \begin{array}{c} -\boldsymbol{J}_1 \\ \cdot \\ \cdot \\ \cdot \\ -\boldsymbol{J}_{n_s} \\ \sigma \\ \boldsymbol{u}^T\sigma - \Sigma_k \boldsymbol{q}^k - \Sigma_s \boldsymbol{J}_s h_s \\ -\boldsymbol{q}^{ve} - \Sigma_s \boldsymbol{J}_s e^{ve} \end{array} \right\}, \boldsymbol{Q} = \left\{ \begin{array}{c} \dot{\omega}_1 \\ \cdot \\ \cdot \\ \cdot \\ \dot{\omega}_{n_s} \\ \boldsymbol{0} \\ 0 \\ \dot{\Theta}^{tr:ve} + \Sigma_s \dot{\omega}_s e_s^{ve} \end{array} \right\} \tag{2}$$

Furthermore, the wall heat flux in SU2-NEMO is computed using the surface energy balance given in Equation (3) [7]

$$q_w = \sum_k \lambda^k \nabla T^k \cdot \boldsymbol{n} + \sum_s \rho_s D_s h_s \nabla c_s \cdot \boldsymbol{n}. \tag{3}$$

The first term in Equation (3) represents Fourier's Law of heat conduction, where the summation is performed over temperature gradient contributions for the energy modes $k \in [tr, ve]$. The second term represents the

contribution due to enthalpy diffusion at the surface. This contribution can be neglected in non-dissociated flows but becomes significant in the presence of large concentration gradients at the wall.

The thermochemical nonequilibrium closure terms $\boldsymbol{Q}$, transport properties, and mixture energies must be calculated in order to close the system of governing equations that describes hypersonic flow. Thermochemistry models are implemented inside SU2-NEMO via linking to the Mutation++ library (Multicomponent Thermodynamic And Transport properties for IONized gases in C++) [8], which provides algorithms for the computation of thermodynamic, chemical kinetics, and transport gas properties. Additionally, SU2-NEMO also includes a native thermochemical library. This enables SU2-NEMO access to a range of nonequilibrium kinetic physical models and the capability to simulate any mixture of gases and mechanisms of reactions.

Two-temperature model

In a gas phase, the energy carried within a polyatomic molecule of different species is distributed among translational, rotational, vibrational, and electronic degrees of freedom. In the models that are implemented in the SU2-NEMO, rotational energy is determined assuming rigid body dynamics (fixed bond length) for polyatomic molecules and vibrational energy is approximated as a simple harmonic oscillator. Coupling between the rotational and vibrational modes due to bond length variation is neglected and the energy modes are assumed to be independent. Separate temperatures are used to track the translational–rotational energy modes and vibrational–electronic energy modes, in order to take into account differences in the number of collisions required to reach equilibrium. This two-temperature model assumes equilibrium between the translational and rotational energy modes, and between the vibrational and electronic modes, but also assumes that these two sets are not necessarily in equilibrium with each other. The rigid-rotor harmonic oscillator (RRHO) two-temperature model has been shown to accurately predict flow and transport properties from high supersonic to atmospheric entry conditions. Through the independence of the energy levels, the total energy and vibrational– electronic energy per unit volume can be expressed as [6]:

$$\rho e = \sum_s \rho_s(e_s^{tr} + e_s^{rot} + e_s^{vib} + e_s^{el} + e_s^{o} + \frac{1}{2}\boldsymbol{u}\boldsymbol{u}^T), \tag{4}$$

and

$$\rho e^{ve} = \sum_s \rho_s(e_s^{vib} + e_s^{el}). \tag{5}$$

If a general gas mixture consisting of polyatomic, monatomic, and free electron species is considered, expressions for the energy stored in the translational, rotational, vibrational, and electronic modes can be represented as

$$e_s^{tr} = \begin{cases} \frac{3}{2}\frac{R}{M_s}T_{tr} & \text{for monoatomic and polyatomic species,} \\ 0 & \text{for electrons,} \end{cases} \tag{6}$$

$$e_s^{rot} = \begin{cases} \frac{\xi}{2}\frac{R}{M_s}T_{tr} & \text{for polyatomic species,} \\ 0 & \text{for monoatomic species and electrons,} \end{cases} \tag{7}$$

where ξ is an integer specifying the number of axes of rotation,

$$e_s^{vib} = \begin{cases} \frac{R}{M_s}\frac{\theta_s^{vib}}{exp(\theta_s^{vib}/T_{ve})-1} & \text{for polyatomic species.} \\ 0 & \text{for monoatomic species and electrons,} \end{cases} \tag{8}$$

where θ_s^{vib} is the characteristic vibrational temperature of the species, and

$$e_s^{el} = \begin{cases} \frac{R}{M_s}\frac{\sum_{i=1}^{\infty} g_{i,s}\theta_{i,s}^{el}exp(-\theta_{i,s}^{el}/T_{ve})}{\sum_{i=0}^{\infty} g_{i,s}exp(-\theta_{i,s}^{el}/T_{ve})} & \text{for polyatomic species,} \\ \frac{3}{2}\frac{R}{M_s}T_{ve} & \text{for electrons,} \end{cases} \tag{9}$$

where θ_s^{el} is the characteristic electronic temperature of the species and g_i is the degeneracy of the ith state. The energy exchange between the translational-rotation and vibrational-electronic modes, $\dot{\Theta}^{tr:ve}$, is modeled using a Landau-Teller formulation with Park high-temperature correction

$$\dot{\Theta}^{tr:ve} = \sum_s \rho_s \frac{de_s^{ve}}{dt} = \frac{e_s^{ve*} - e_s^{ve}}{\tau_s}, \tag{10}$$

where τ_s is computed using a combination of the Landau–Teller relaxation time, $\langle\tau_s\rangle_{L-T}$, and a limiting relaxation time from Park, τ_{ps}. More detail about this formulation in SU2-NEMO can be found in [6].

Finite-rate chemical kinetics

The presence of energetic collisions also results in chemical reactions occurring in the flow. In Equation (2), the source terms in the species conservation equations are the species volumetric mass production rates, which are governed by the forward and backward reaction rates, R^f and R^b, for a given reaction r, and can be expressed as [6]

$$\dot{\omega}_s = M_s \sum_r (\beta_{s,r} - \alpha_{s,r})(R_r^f - R_r^b). \tag{11}$$

From kinetic theory, the forward and backward reaction rates are dependent on the molar concentrations of the reactants and products, as well as the forward and backward reaction rate coefficients, k^f and k^b, respectively, and can be expressed as

$$R_r^f = k_r^f \prod_s (\frac{\rho_s}{M_s})^{\alpha_{s,r}}, \tag{12}$$

and

$$R_r^b = k_r^b \prod_s (\frac{\rho_s}{M_s})^{\beta_{s,r}}. \tag{13}$$

For an Arrhenius reaction, the forward reaction rate coefficient can be computed as

$$k_r^f = C_r(T_r)^{\eta_r} exp(-\frac{\epsilon_r}{k_B T_r}), \tag{14}$$

where C_r is the pre-factor, T_r is the rate-controlling temperature for the reaction, η_r is an empirical exponent, and ϵ_r is the activation energy per molecule. The backward reaction rates k_r^b are determined from the equilibrium reaction rates $k_r^b = k_r^f / k_r^{eq}$, for every reaction r. The equilibrium reaction rates k_r^{eq} are determined as a function of the Gibbs free energy.

Transport properties

Mass, momentum, and energy transport in fluids are all governed by molecular collisions, and expressions for these transport properties can be derived from the kinetic theory. The mass diffusion fluxes, $\boldsymbol{J}_s$, are computed using Fick's Law of Diffusion:

$$\boldsymbol{J}_s = \rho D_s \nabla(c_s), \tag{15}$$

where c_s is the species mass fraction and D_s is the species multi-component diffusion coefficient. The values of D_s are computed as a weighted sum of binary diffusion coefficients between all species in the mixture. These are obtained by solving the Stefan–Maxwell equations under the Ramshaw approximations [6]. The viscous stress tensor is written as

$$\boldsymbol{\sigma} = \mu(\nabla \boldsymbol{u} + \nabla \boldsymbol{u}^T - \frac{2}{3}\boldsymbol{I}(\nabla \cdot \boldsymbol{u})), \tag{16}$$

where μ is the mixture viscosity coefficient. The conduction heat flux for each thermal energy mode, $\boldsymbol{q}^k$, is assumed to be given by Fourier's Law of heat conduction:

$$\boldsymbol{q}^k = \lambda^k \nabla(T^k), \tag{17}$$

where T^k is the temperature and λ^k is the thermal conductivity coefficient of the kth energy mode. Viscosity and thermal conductivity are computed using Wilke's mixing rule [9]. The species viscosity model is calculated using either Blottner's three-parameter curve fits for high-temperature air [10], or Gupta–Yos [11]. Thermal conductivity is calculated using Eucken's formula [12].

Gas-Surface interaction

In dissociated flows, catalytic recombination at the wall can be a significant contributor to overall thermal loads. Mechanisms of gas-surface interaction (GSI) are implemented as specific boundary conditions within the SU2-NEMO computational suite. Wall-catalyzed reactions occurring at the surface are modeled by the production of chemical species due to catalytic reactions, $\dot{\omega}^{cat}$, that must be balanced by the normal diffusive and convective flux at the wall. For steady flow and a no-slip boundary, this can be expressed as [13]

$$\boldsymbol{J}_s \cdot \boldsymbol{n} = \dot{\omega}_s^{cat}. \tag{18}$$

When computing the viscous component of the residual in SU2-NEMO, the chemical production of species due to catalytic processes is taken into account as an extra diffusive flux that is equivalent to the chemical source term computed due to catalytic reactions. Gradients of species density are then computed directly as part of the SU2-NEMO computational routine, which are used to compute gradients of species mass fraction at wall vertices. A super-catalytic wall option in SU2-NEMO allows for the specification of full recombination to a given equilibrium concentration (usually the free-stream conditions) [7].

$$c_{w,s} = c_{eq,s}. \tag{19}$$

While there is no physical mechanism to enforce full recombination, the supercatalytic boundary is a useful analysis tool, in that it provides a conservative upper bound on surface heating augmentation due to recombination. Other option include a partial catalytic wall which is implemented using gamma model [7]

$$\dot{\omega}_s^{cat} = \gamma_s c_s \rho_w \sqrt{\frac{R_s T_w}{2\pi}}, \tag{20}$$

where γ_s is the species catalytic efficiency, and represents the proportion of incident mass flux of monatomic species which recombines into its heteronuclear diatomic molecule at the wall. The catalytic efficiency is strictly confined to the interval $\gamma_s \in [0,1]$, with a value of zero corresponding to a noncatalytic surface, and a value of 1 corresponding to a fully-catalytic surface. In the time when work was being performed, taking into account surface catalytic effects was not possible for the mixture model of the Martian atmosphere.

Turbulence Modeling

As mentioned before, the aerothermal loads are critical to the design of the TPS, the shape of the vehicle, and the allowable materials that can be used. The presence of a turbulent boundary layer can significantly augment the surface heat load, particularly for low-altitude, endoatmospheric flight. While many turbulence models exist, the field continues to be highly studied, particularly for hypersonic flows. For these flows, modeling inconsistencies still hamper the prediction of surface temperatures and heat flux, which can result in significant design uncertainties. As such, SU2-NEMO enables the use of several standard turbulence models, including the Spalart-Almaras (SA) and the Shear-Stress-Transport (SST) models. SU2-NEMO also employs several modifications to these standard models [13]. Currently, turbulent non-equilibrium flow models are not available, but work is being performed in order to incorporate them.

2.2.   Numerical Implementation

In this section numerical implementation of models within SU2-NEMO are presented. This includes both the numerical schemes for discretization of the governing equations and time-integration strategies. The basic numerical procedures are consistent with those implemented in the base SU2 software, for more detail, refer to Reference [5]. However, inside SU2-NEMO, some specific convective schemes well-suited for simulation of high-speed flows are implemented, which are described in more detail in the following discussion.

2.2.1   Spatial Integration

Within the SU2, the discretized governing equations are solved using the Finite Volume Method on an edge-based median dual-grid numerical mesh. For a control volume Ω_i the discretized conservation equations can be written as

$$\int_{\Omega_i} \frac{\partial \boldsymbol{U}_i}{\partial t} d\Omega + \sum_{j \in N(i)} (\hat{\boldsymbol{F}}_{ij}^c + \hat{\boldsymbol{F}}_{ij}^v)\Delta S_{ij} - \boldsymbol{Q}|\Omega_i| = \int_{\Omega_i} \frac{\partial \boldsymbol{U}_i}{\partial t} d\Omega + \boldsymbol{R}(\boldsymbol{U}_i) = 0, \tag{21}$$

where $\boldsymbol{U}_i$ is the vector of conservative variables and $\boldsymbol{R}(\boldsymbol{U}_i)$ is the residual representing the integration of all spatial terms at node i. $\hat{\boldsymbol{F}}_{ij}^c$ and $\hat{\boldsymbol{F}}_{ij}^v$ are the numerical approximations of the convective and viscous fluxes, and $\boldsymbol{Q}$ is a vector of source terms. ΔS_{ij} is the area of the face associated with the edge ij, Ω_i is the volume of the dual control volume, and $N(i)$ is the set of neighboring nodes to node i. The convective and viscous fluxes are computed at the midpoint of each edge and added/subtracted to the residual for each of the two nodes making up a particular edge [6].

Convective Flux

Convective fluxes can be discretized using upwind and central convective schemes. In the framework of SU2-NEMO, the emphasis is on two schemes implemented specifically for high-speed flow simulation: the Modified Steger-Warming (MSW) and Advection Upstream Splitting Method (AUSM) flux-vector splitting schemes [6].

An upwinding numerical technique called the original Steger-Warming flux-vector splitting algorithm is used to resolve flows in the presence of strong shocks. The scheme entails dividing the flux vector according to how information spreads across the flow. Due to MSW's highly dissipative properties, which mitigate the stiffness of nonequilibrium equations' effect on convergence, it is commonly employed. Modified Steger-Warming adds a weighting factor to reduce numerical dissipation in the presence of strong pressure gradients, such as near-shocks and in boundary layers, to address accuracy concerns of the Steger-Warming scheme and to assure greater accuracy without compromising flow stability [6].

Another popular flux-vector splitting technique for high-speed flows is AUSM. The scheme divides the flux vector into terms propagating at the local sound speed and terms propagating at the local flow velocity. The AUSM scheme is more precise and reliable than MSW and has less numerical dissipation. In addition to the above-mentioned scheme, SU2-NEMO also includes a number of AUSM extensions. These include the AUSM+M and AUSM+up2 schemes, which have been enhanced versions of the original AUSM scheme's stability and precision. The AUSM family of schemes provides better shock capture and avoids the presence of carbuncles, which are seen in stagnation areas surrounding blunt bodies. Like the base SU2 code, SU2-NEMO features slope-limiters for solutions with higher-order precision [6].

Viscous Flux

Viscous flux values are computed at the median dual-grid interfaces. Information about the gradient required for the viscous fluxes can be evaluated by either the Gauss-Green Theorem or Weighted Least-Squares approach, with appropriate corrections in areas of high cell skewness [6].

2.2.2 Time Integration

With explicit time integration (explicit forward Euler and Runge-Kutta explicit) and implicit time integration (implicit backward Euler), SU2-NEMO makes use of the time integration capabilities offered by the overall SU2 framework. Since explicit time integration systems require a local update at each cell, they are simple to parallelize. The disadvantage is that explicit systems impose limitations on the local time-step's permitted Courant-Friedrichs-Lewy (CFL) number based on wave speed. A considerable number of iterations may be necessary for the CFL number to converge, particularly in areas with significant gradients. Implicit techniques do not experience the same stability issues as explicit techniques because they absorb information at the next time-step. However, they demand that all residual equations be solved simultaneously [6].

2.3. Boundary Conditions

SU2-NEMO employs several wall boundary conditions similar to those in the base SU2 code. These include non-catalytic isothermal and heat flux wall boundaries for viscous flow simulation, as well as the inviscid Euler wall. The Smoluchowski–Maxwell boundary condition is also implemented for modeling rarefied flows. Surface-catalyzed chemical reactions can have a significant impact in high-speed flows, and in SU2-NEMO this is taken into account through super-catalytic and partially-catalytic wall boundary conditions [14].

3. Validation Cases

SU2-NEMO is a recent extension of the SU2 software. For this reason, the number of validation cases present in the literature is limited. In this section, two validation cases are investigated in order to prove SU2-NEMO's capability of dealing with complex physics involved in entry vehicle flowfields. In both cases, the MSL entry vehicle is used as a test case. First, geometry and the computational domain are presented, followed by the results and discussion of numerical simulation.

3.1.   Geometry and Computational Domain

As mentioned before, MSL entry vehicle is used as a test case for the analysis. The shape of MSL entry vehicle is derived from previous NASA missions to Mars. The heatshield is based on a blunted nose cone with a half angle of 70-degree, with a nose radius 1/2 of the vehicle's base radius. The backshell is a series of truncated cones, sized in such a way as to accommodate the payload. The outer surface contains features and components such as cruise and entry balance masses, which are not always flush, and is therefore more complex than simply a collection of spherical, conical and toroidal surfaces [1]. For the purposes of this analysis, the shape is simplified as shown in Figure 1.
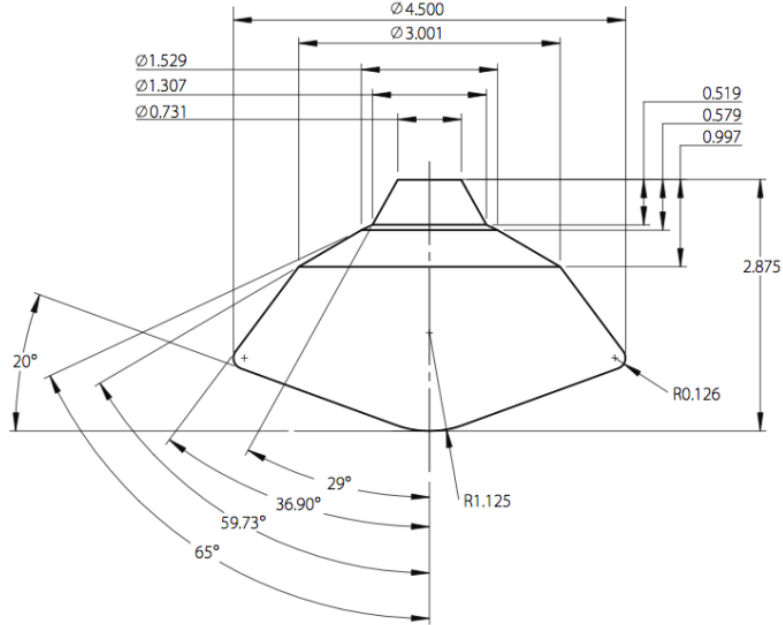
Figure 1: Simplified MSL geometry [1].

Solutions were obtained on a 7-block singularity-free grid. The computational grid was constructed using the GMSH software. For the purpose of this work, only the forebody of the capsule is considered, similarly to the literature, [1, 15]. The heatshield nose was meshed in such a way as to avoid a singularity pole boundary because this can lead to discontinuities in the flowfield solution. Figure 2 shows the surface and symmetry plane grid distributions with the corresponding boundary conditions. Only half of the heatshield is modeled because of symmetry in the pitch plane. In order to resolve the flowfield, 6400 surface and 128 normal cells was used, making in total 819200 volume elements.

3.2.   Computational Approach

Navier-Stokes solutions of the MSL flowfield at flight conditions have been generated using the SU2-NEMO CFD code. For Mars flight conditions, SU2-NEMO is coupled with the 8- species Mars gas model (CO_2, CO, N_2, O_2, NO, C, N, O) in chemical and thermal non-equilibrium using the Park-94 reaction rates [16]. Since the native SU2 library does not support this gas model, the Mutation++ library, a well-validated physio-chemical library, is used in order to create the required Mars 8-species gas model. This model is the original contribution of the author of this work, since before there was no existence of such a model available in the Mutation++ database [17]. For more details regarding the Mars 8-species gas model refer to Appendix A. The mixture dynamic viscosity and thermal conductivity are computed using Wilke's semi-empirical mixing rule. The species viscosity model is calculated using Blottner's three-parameter curve fits and the species thermal conductivities are computed according to Eucken's formula. As a convective flux scheme, advective upstream splitting (AUSM) method is used since it has a good shock-capturing capability. Viscous fluxes are discretized at the median dual grid interfaces and the Weighted Least Squares algorithm is used for gradient calculation. A finite-volume approach is used to solve the full Navier-Stokes flowfield equations for all calculations presented here. Constant inflow condition was imposed using the farfield boundary condition, and the extrapolation was used on the outlet boundary in all solutions. An isothermal non-catalytic wall with $T_w = 300K$ is implemented for the heatshield surface. Symmetry boundary condition is used for the symmetry plane. The flowfield is assumed to be steady and laminar.
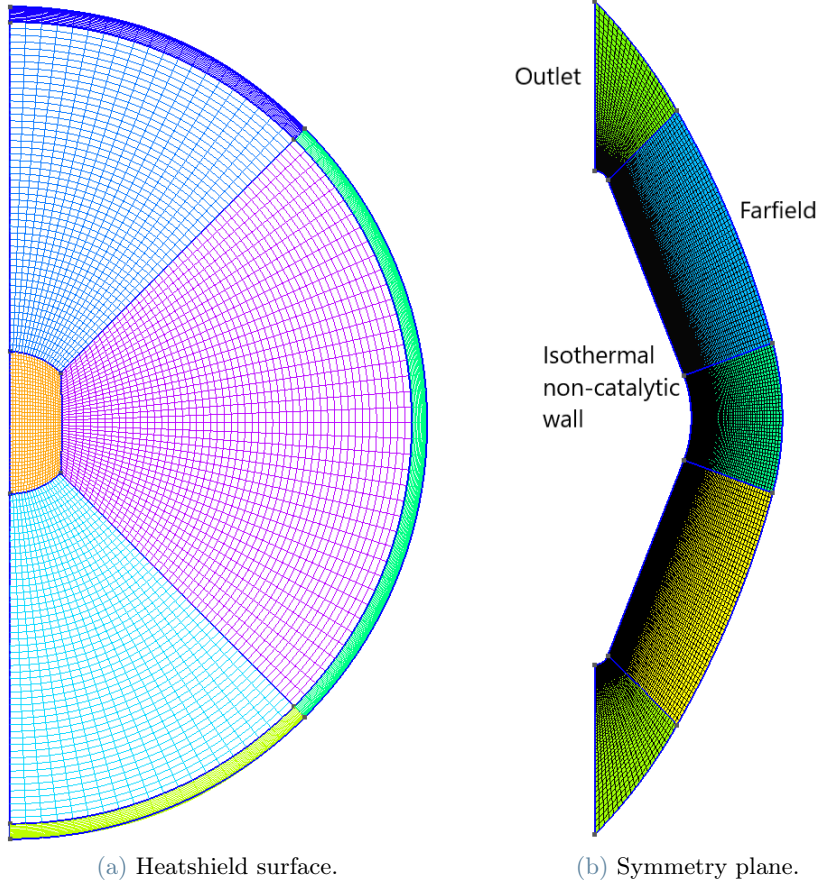
(a) Heatshield surface.　　　(b) Symmetry plane.

Figure 2: Heatshield surface and symmetry plane grids.

3.3.　Validation Case 1

The first validation case is used to replicate results from the MSL Aerodynamic Database (ADB) [1]. The specific point along the 05-22 nominal trajectory was selected in order to validate the capabilities of SU2-NEMO. Since the MSL vehicle is designed to achieve a hypersonic lift-to-drag (L/D) of 0.24 at the trimmed angle of attack of 16°, for the purpose of the analysis, a point along the trajectory with the angle of attack of 16° is selected. Freestream conditions used for CFD solution are given in Table 1. Note, the composition of the gas in Table 1 is expressed in terms of mass fractions.

$\rho_\infty(kg/m^3)$	$T_\infty(K)$	$V_\infty(m/s)$	$c[CO_2]_\infty$	$[CO]_\infty$	$[N_2]_\infty$	$[NO]_\infty$	$[CO_2]_\infty$	$[C]_\infty$	$[N]_\infty$	$[O]_\infty$
3.483E-03	189.4	2000	0.97	0	0.03	0	0	0	0	0

Table 1: Freestream Conditions for Validation Case 1.

3.3.1　Results

Hypersonic flow over a blunt body such as MSL is computationally challenging due to the complex physics involved. Figure 3 shows Mach number distribution in a flowfield along the symmetry plane, with the solution obtained using the SU2-NEMO CFD code. As can be seen from Figure 3, a strong bow shock wave is detached from the surface and lies very close to the heatshield. At an angle of attack of 16°, the heatshield stagnation point moves from the spherical nose onto the "windside" section. Furthermore, in Figure 4a pressure distribution along the symmetry plane is presented (left), while the normalized pressure distribution along the heatshield surface is shown on the right. Normalized pressure is obtained using $p/\rho_\infty v_\infty^2$. In Figure 4a, it can be seen that the pressure over MSL is highest at the heatshield stagnation point and drops rapidly as the flow expands around the shoulder pivot point. For comparison, in Figure 4b computational results, at the same angle of attack of 16°, using NASA LAURA CFD code are also shown [15]. Figure 4b clearly shows that the complex

physics of the hypersonic flow over the blunt body is very well captured using the SU2-NEMO. Shock wave position and shape are well resolved. Also, pressure flowfield and surface distributions computed using SU2-NEMO and LAURA CFD code are in good agreement. It should be noted that results in Figure 4 are obtained using different freestream conditions. Furthermore, in Table 2, results concerning axial (C_A) and normal (C_N) aerodynamic coefficients are shown, as well as hypersonic lift-to-drag ratio (L/D). In Table 2, the results of the SU2-NEMO CFD code are compared with the results present in the ADB for the same freestream conditions. Moreover, lift (C_L) and drag (C_D) coefficients are extracted from C_A and C_N using the following relations:

$$C_L = C_A \sin \alpha + C_N \cos \alpha, \tag{22}$$
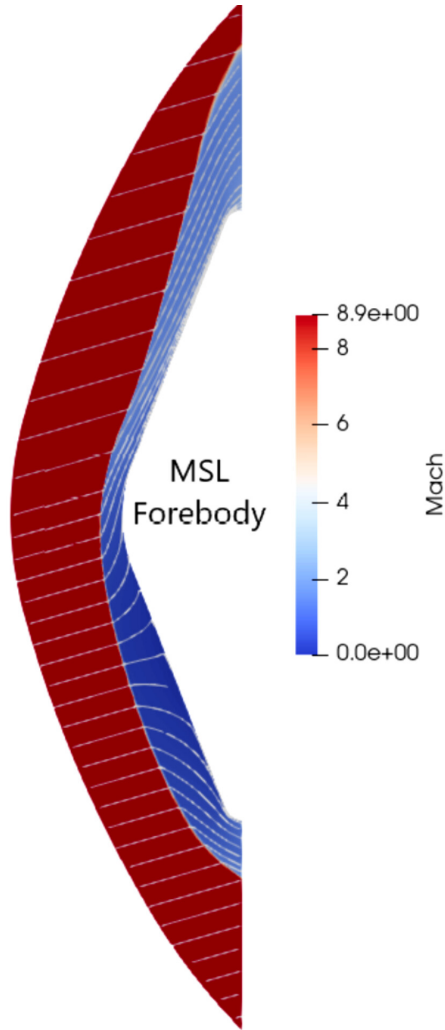
and

$$C_D = C_A \cos \alpha + C_N \sin \alpha. \tag{23}$$

Figure 3: Hypersonic flowfield over MSL capsule.

(a) SU2-NEMO results
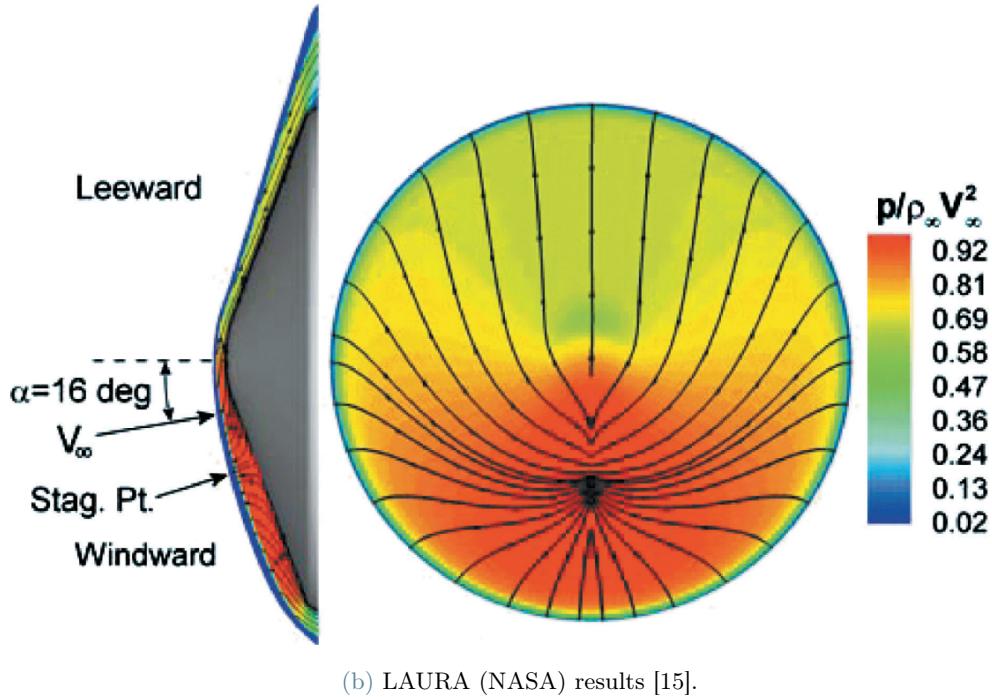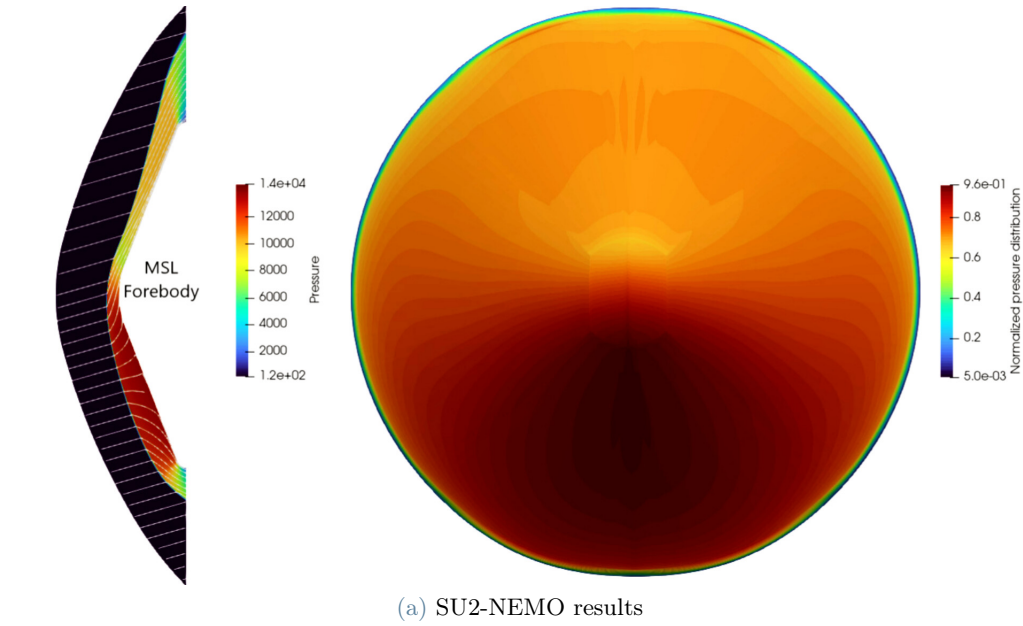

(b) LAURA (NASA) results [15].

Figure 4: Flowfield code to code comparison.

In general, there is a good agreement between the results obtained using the SU2-NEMO CFD code and the results available in ADB. The designed lift-to-drag ratio of 0.24 at an angle of attack of $\alpha = 16°$ is also obtained using SU2-NEMO, while some minor differences exist in the C_A and C_N. Therefore, it can be concluded that the SU2-NEMO CFD code is able to accurately predict mechanical loads acting on the MSL entry vehicle in a hypersonic regime.

CFD Code	C_A	C_N	C_D	C_L	L/D
SU2-NEMO	1.492	5.704E-02	1.450	0.356	0.245
LAURA (ADB)	1.478	4.744E-02	1.433	0.361	0.251

Table 2: Comparison of aerodynamic characteristics [1].

3.4. Validation Case 2

Even though it is shown in the previous section that SU2-NEMO is capable of accurately calculating mechanical loads and corresponding aerodynamic coefficients, in ADB [1], there is no data related to the aerothermodynamic environment (heat flux, surface pressure, and surface shear stress) encountered by MSL capsule at a specific point along the trajectory. For that reason, the author performed another validation case in order to confirm that SU2-NEMO coupled with the Mutation++ library can accurately reconstruct the aerothermodynamic environment available in the literature, [18]. In this case, freestream conditions used for CFD solution are given in Table 3. This time angle of attack is 18.2°. Note, that again, the composition of the gas in Table 3 is expressed in terms of mass fractions.

| $\rho_\infty(kg/m^3)$	$T_\infty(K)$	$V_\infty(m/s)$	$[CO_2]_\infty$	$[CO]_\infty$	$[N_2]_\infty$	$[NO]_\infty$	$[CO_2]_\infty$	$[C]_\infty$	$[N]_\infty$	$[O]_\infty$
2.86E-03	204	2510	0.97	0	0.03	0	0	0	0	0

Table 3: Freestream Conditions for Validation Case 2.

3.4.1 Results

Hypersonic flowfield has the same structure as presented in Figure 3. In Figure 5, the aerothermodynamic environment along the symmetry plane cut obtained using the SU2-NEMO code is compared with the NASA LAURA CFD code [18]. In Figure 5a heat flux along the the symmetry plane cut is shown. MSL capsule is the first capsule that experienced turbulent conditions at the time of peak heating. It is known that turbulent conditions increase the magnitude of both heat flux and shear stress. This is very important to consider in order to properly design a thermal protection system (TPS). The previous discussion is relevant since from Figure 5a it can be seen that moving away from the stagnation point of the capsule, there are noticeable differences in predicted heat flux. The difference is the highest at the leeside of the capsule, where turbulent boundary layer is fully resolved. The main reason is that SU2-NEMO at the time of analysis, was not able to take into account turbulent conditions within the framework of thermochemical non-equilibrium flows at high Mach number. The same conclusion was obtained in the original paper, where calculations were run with both laminar and turbulent conditions, [18]. Furthermore, another difference in the predicted heat flux comes from the fact that in the original paper, the super-catalytic wall boundary condition was implemented to fix the mass fractions of CO_2 and N_2 to their freestream values of 0.97 and 0.03, respectively. This boundary condition results in conservative heating predictions in flight, while in SU2-NEMO, this condition is available only for some gas mixtures. For this reason, using a non-catalytic isothermal wall boundary results in an underprediction of heat flux since exothermic chemical reactions that occur near the wall are not taken into account. Furthermore, in Figure 5b, pressure distribution along the symmetry plane cut is shown. There is a good agreement between the two codes. This is due to the fact that pressure distribution is not influenced by the turbulent boundary layer, which is confirmed in the original paper, [18]. Lastly, Figure 5c presents the shear stress distribution along the symmetry plane cut. Again, a similar discussion is valid, like in the case of the heat flux, turbulent conditions augment shear stress, and that is the reason for the noticeable difference in the two codes, especially in the leeside flank. To conclude, the results of this validation case prove SU2-NEMO CFD code capability of modeling high Mach number flows in thermochemical non-equilibrium. The SU2-NEMO developer team is currently working on the development of turbulent models within the NEMO framework, which will make SU2-NEMO an even more reliable tool for the analysis of the aerothermodynamic environments of entry vehicles.
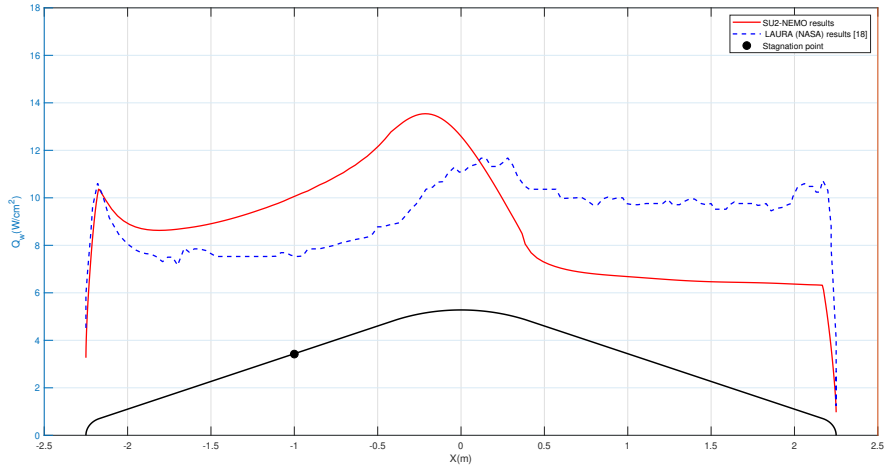
(a) Heat flux profile along the symmetry plane cut.
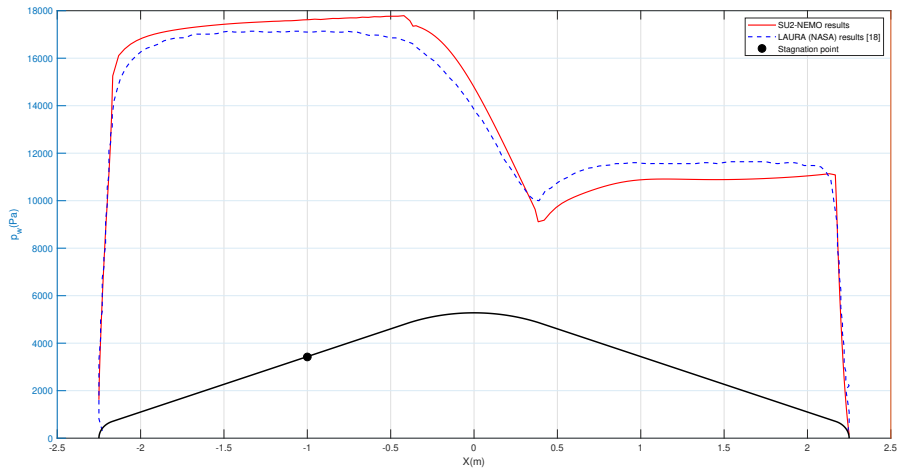
(b) Pressure profile along the symmetry plane cut.
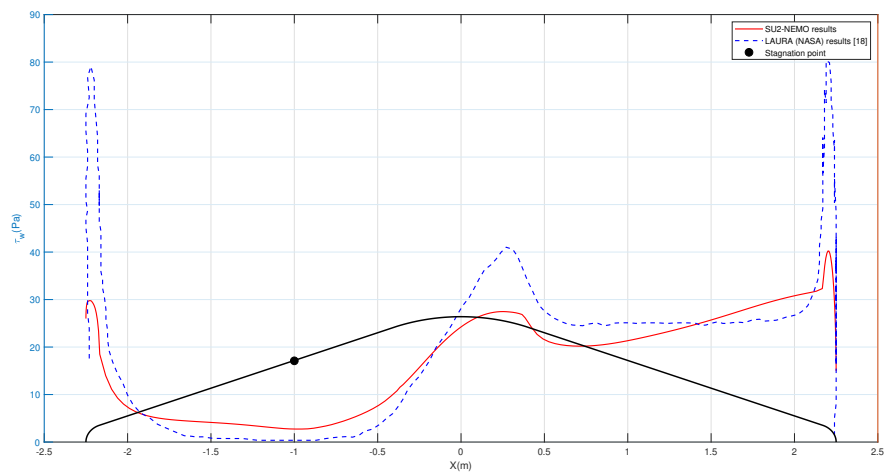
(c) Shear stress profile along the symmetry plane cut.

Figure 5: Aerothermodynamic environment of MSL capsule.

4. Parametric study

As stated before, this research will focus on one possible way to eliminate the problem of descending and landing on Mars's surface. In particular, to increase the deceleration of the vehicle at higher altitudes, the vehicle's drag coefficient must be increased. Several researches concerning the shape optimization for the forebody of the entry capsule using detailed CFD analyses [19, 20] and Newtonian flow formula [21] are available. However, these optimum shapes were changed drastically from the shape of the current entry capsule. If the shape of the capsule was changed drastically, then it is necessary to confirm the efficacy of the updated design, and this is not so cost effective. In other words, it is helpful to improve the aerodynamic characteristics by a slight modification of the shape. One of the possible approaches available in the literature is by using hyperbolic curves [4]. The forebody contours of the most re-entry vehicles are based on the blunted nose cone, and they are determined by a combination of the arc and the inclined line. Also, this type of contour can be approximated by using hyperbolic curves. This section investigates aerodynamic characteristics and the aerothermodynamic environment of the re-entry capsule with a forebody designed using hyperbolic curves.

4.1. Forebody Design Using Hyperbolic Contours

For the purpose of the analysis, MSL entry vehicle will be used as a test case. The shape of the MSL's forebody is presented in Figure 1. The approach used in order to modify the forebody of the capsule is as follows. First, the contour of the MSL forebody up to the shoulder pivot point (Figure 6) is approximated by the following hyperbola:

$$(\tan (s))^2 (x + a)^2 - y^2 = (\tan (s))^2 (x_{pp}^2 + 2x_{pp}a + a^2) - y_{pp}^2, \tag{24}$$

where s represents the slope of the hyperbola in degrees, and x_{pp} and y_{pp} represent x and y coordinates of the shoulder pivot point. Equation (24) represents hyperbola through the shoulder pivot point for a given slope s, irrespective of the parameter a. In order to achieve a smooth transition from hyperbolic contour to the shoulder region (Figure 6), the shoulder region is modified by changing the angle of the circle arc from the shoulder pivot point to the end of the shoulder region. The 3D shape of the forebody of the modified capsule is created as a hyperboloid of revolution around the X axis. Several combinations of a and s were tested, and they are represented in Figure 6. These combinations are obtained by trial and error method in order to find combinations of s and a, which can best replicate the forebody shape of the original MSL capsule. As can be seen from Figure 6, when $s = 68.5°$ and $a = 0.977$, MSL's original shape is very well approximated using the hyperbolic contour. For this reason, the slope of the hyperbola is selected to be 68.5°, while parameter a will be varied in order to see how the change in the shape will influence aerodynamic characteristics as well as the aerothermodynamic environment.
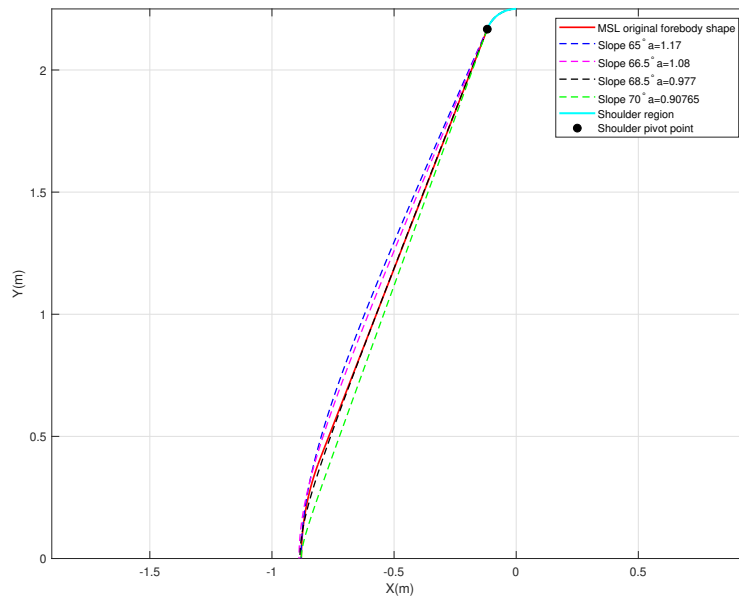

Figure 6: Shapes of the forebody with hyperbolic contours.

4.2.   Forebody Geometries and Computational Approcah

As stated in the previous section, the slope of the hyperbola is selected to be 68.5°. For the purpose of the analysis, parameter a is gradually increased for the same value of the slope. As a consequence, this leads to a decrease in the overall volume of the capsule forebody, which can be seen in Figure 7. For comparison, in Figure 7, the original forebody of the MSL capsule is also depicted. The reason for increasing the parameter a and hence reducing the overall volume is due to the investigation performed in [4], where it was proved that a decrease in the volume of the forebody of the capsule leads to an increase in the drag coefficient. Therefore, analysis will be performed to investigate whether this type of approach will have a positive impact. It should be noted that the reference area for all geometries is equal to the original MSL capsule. The computational domain is constructed in a similar manner to the one presented in Section 3.1. Again, GMSH software is used to create 3D volume. A 7-block singularity-free grid is used to avoid any possible numerical discontinuities. Figure 8 shows the grid distribution along the heatshield surface and symmetry plane. Half of the heat shield is modeled due to symmetry in the pitch plane. To properly resolve the flowfield, 6320 surface, and 128 surface normal cells were used, making in total 808960 volume elements. It should be noted that the computational domain represented in Figure 8 is for the hyperbolic contour when $a = 0.977$ and $s = 68.5°$, but the same approach is also used for the remaining two geometries given in Figure 7. Concerning the physical and numerical models as well as boundary conditions used for the purpose of the analysis, the approach is the same as described in Section 3.2. In order to investigate the aerodynamic characteristics as well as the aerothermodynamic environment of the entry vehicle characterized by the hyperbolic contours, freestream conditions used are given in Table 3. These conditions were used since results for the original MSL capsule have already been validated. Hence, these results will be used as a benchmark to investigate the characteristics of the capsules whose forebody shape is designed using hyperbolic contours.
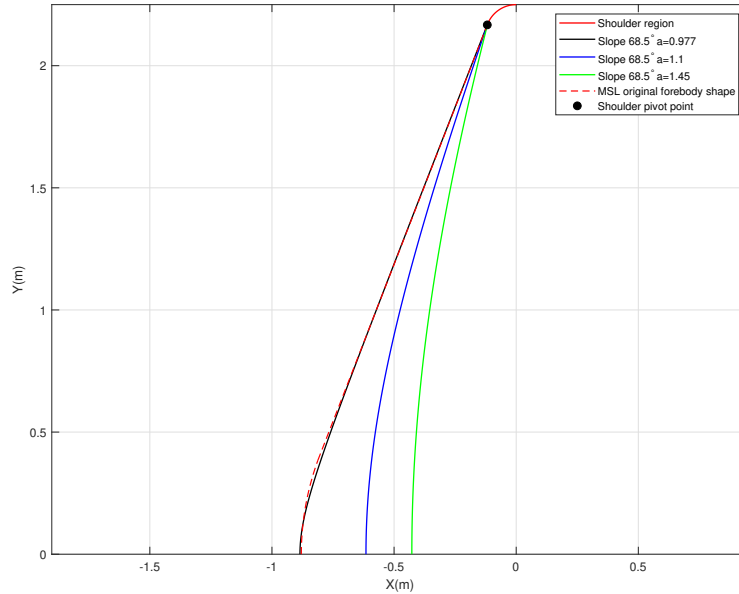

Figure 7: Shapes of the forebody obtained varying parameter a using the same slope.
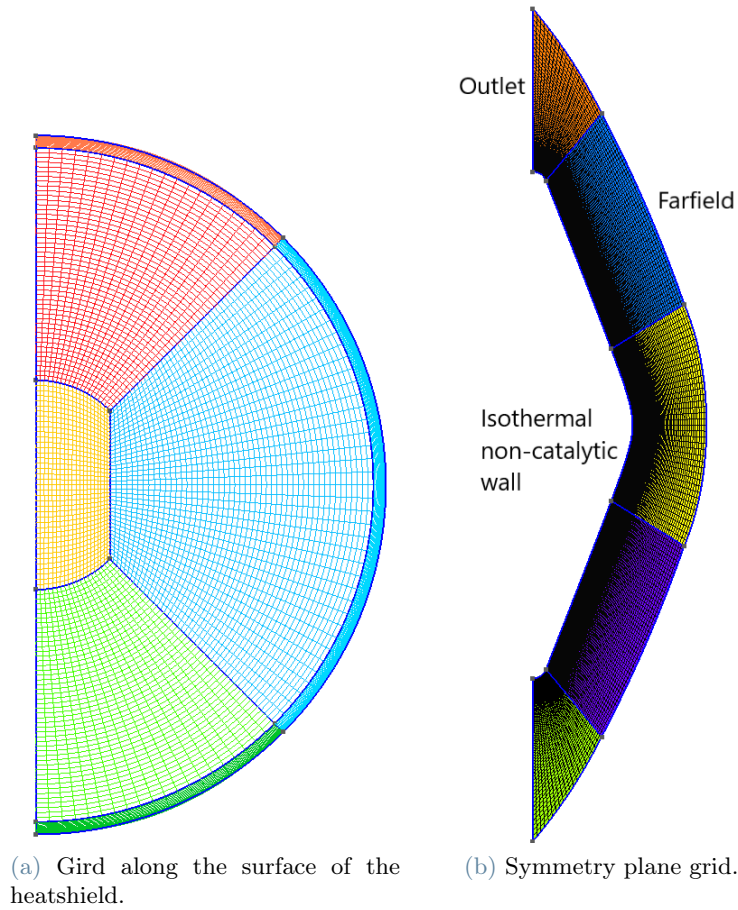
(a) Gird along the surface of the heatshield.

(b) Symmetry plane grid.

Figure 8: Computational grid along the heatshield surface and symmetry plane.

4.3. Results

The comparison between different hypersonic flowfields around selected geometries constructed using hyperbolic contours can be seen in Figure 9. As can be seen in Figure 9, all three geometries have different shapes of the shock layer. This is expected since the shape of the shock is highly influenced by the geometry of the capsule. Moreover, strong bow shock has different shock stand-off distances. Shock is closest to the heatshield in the case of the $a = 0.977$ and its distance increases as the parameter a increases since the radius of the nose increases and overall forebody geometry becomes more blunted.
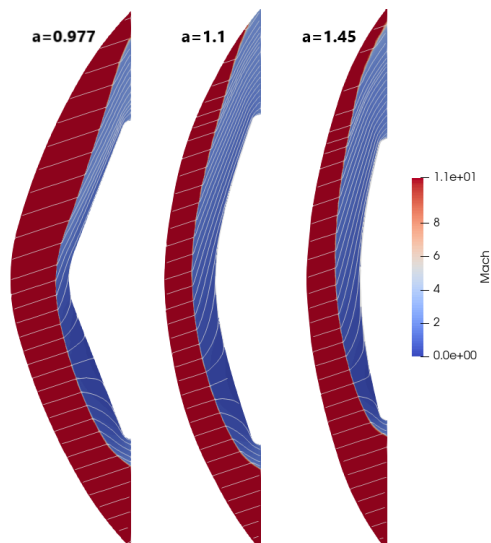

Figure 9: Hypersonic flowfields over entry vehicles characterized with hyperbolic contours.

4.3.1 Aerodynamic Characteristics

The aerodynamic characteristics of entry vehicles characterized by hyperbolic contours are summarized in Table 4. Table 4 shows the comparison of the drag coefficients for hyperbolic contours with the original MSL capsule. From Table 4, it can be observed that only a slight increase in drag coefficients is present when $a = 0.977$ due to very similar geometry to the original MSL capsule. However, as Table 4 suggests, as parameter a increases, the drag coefficients of the capsules which forebody is designed using hyperbolic contours become significantly larger than that of the original MSL capsule at given freestream conditions and angle of attack of 18.2°. This result suggests that the drag coefficient can be increased using hyperbolic contours. This means that for the same mass and reference area, a ballistic coefficient can be reduced. As a result, entry vehicles can be decelerated at higher altitudes, which in turn reduces heat flux [4]. Furthermore, Table 4 shows the comparison of the lift coefficients for hyperbolic contours. From Table 4, it can be observed that when the parameter $a = 0.977$, the lift coefficient is almost the same as the original MSL shape, which is again expected due to very similar geometry. However, as the parameter a increases, the lift coefficient increases as well. These results suggest that the lift coefficient can also be increased using the hyperbolic contours.

	$a = 0.977$	$a = 1.1$	$a = 1.45$	MSL original shape
C_D	1.3993	1.4557	1.5176	1.3990
C_L	0.3865	0.4286	0.4681	0.3868

Table 4: Comparison of drag and lift coefficients using hyperbolic contours to the original MSL shape.
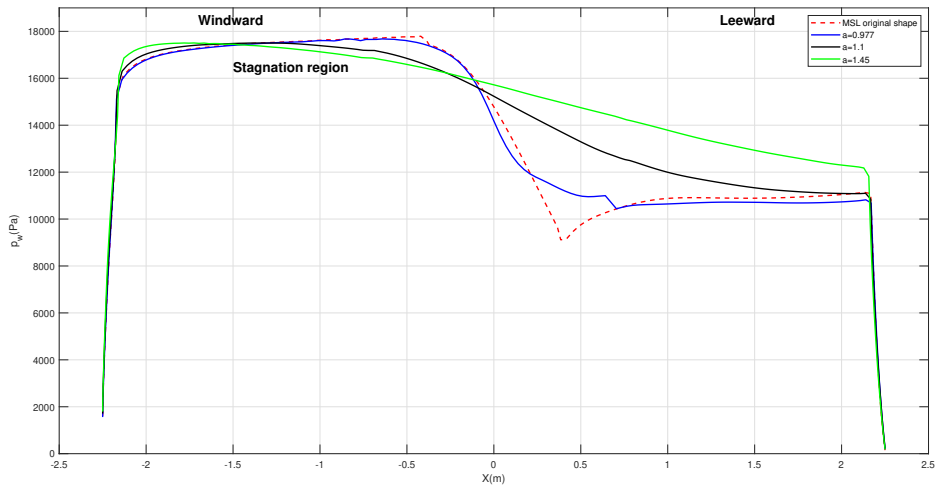
4.3.2 Aerothermodynamic Environment

In order to better understand the aerothermodynamic environment encountered during the hypersonic flight of entry vehicles characterized by the selected forebody geometries, in Figure 10, heat flux, pressure, and shear stress distribution along the symmetry plane cut are presented. From Figure 10a, it can be observed that heat flux in the stagnation region decreases as the parameter a increases. This is expected since heat flux around the stagnation point is lower for more blunted bodies. Furthermore, from Figure 10a it can be seen that on the leeward section of the capsule, heat flux is greater for capsules characterized with $a = 0.977$ and $a = 1.1$ with respect to the original one. Another aspect to consider is pressure distribution along the symmetry plane, Figure 10b. As can be seen from Figure 10b, pressure values are very similar on the windward section of the capsule, especially around the stagnation region. However, on the leeward side, there are noticeable differences. From Figure 10b, it can be deduced that, as the parameter a increases, pressure drop in the leeward section becomes gradual, which means that the leeward section is characterized by higher pressure values. Finally, shear stress along the symmetry plane is depicted in Figure 10c. As can be seen in Figure 10c, around the stagnation region shear stress increases as the parameter a increases. However, the opposite is true on the leeward side, where shear stress becomes significantly lower for the higher values of the parameter a. The previous discussion is particularly important for the sizing of the thermal protection system because forebody ablation can affect aerodynamic stability.

In general, it can be concluded that as parameter a increases, the volume of the capsule and the heat flux transferred to the capsule decrease. This means that from the viewpoint of the volume, the parameter a should be small. However, from the viewpoint of the heat flux, and aerodynamic characteristics, the larger value of the parameter a is beneficial. This implies that the shape of the entry vehicles with hyperbolic contours can be optimized by trading the aerodynamic characteristics, heat flux, and the volume of the capsule.
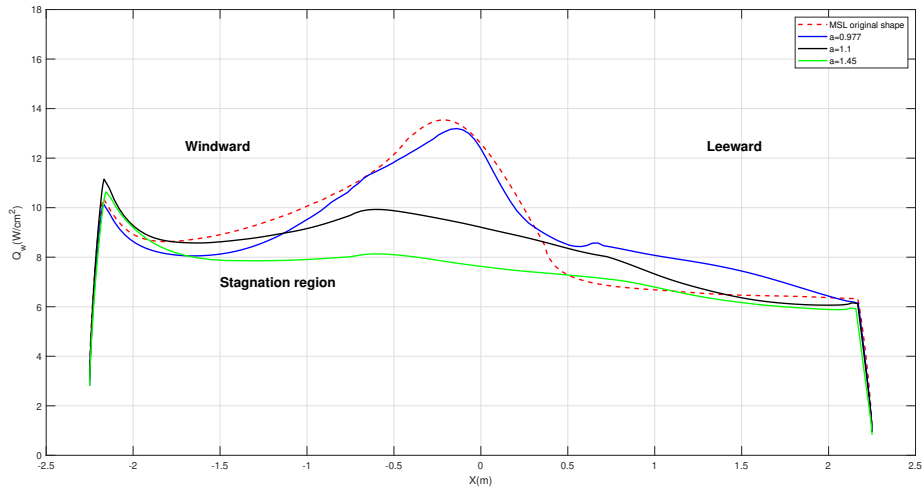
(a) Heat flux profile along the symmetry plane cut.

(b) Pressure profile along the symmetry plane cut.
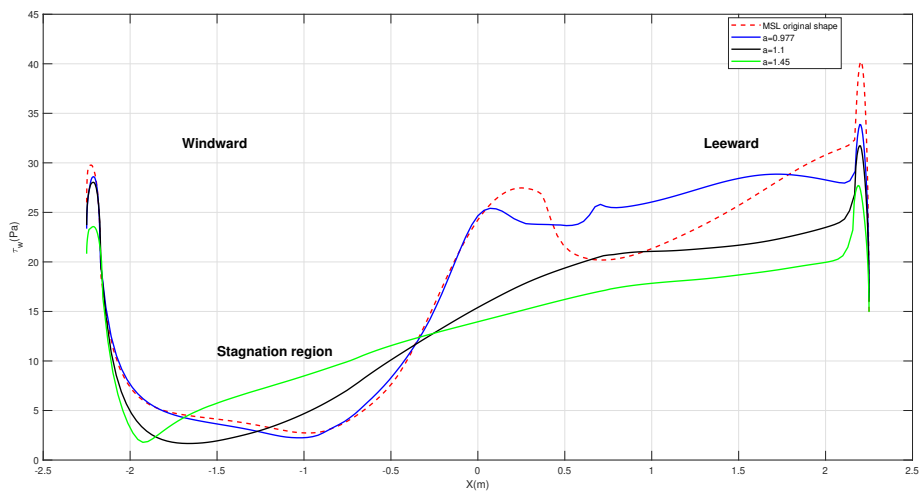
(c) Shear stress profile along the symmetry plane cut.

Figure 10: Comparison of the aerothermodynamic environment of entry vehicles characterized by different shapes of the forebody.

5. Conclusions

In this work, analysis of static aerodynamics and the aerothermodynamic environment of MSL entry vehicle is performed by means of the SU2-NEMO CFD code. Two validation cases were used in order to prove the capability of the SU2-NEMO to accurately simulate hypersonic flow in the Martain atmosphere. Results obtained using the SU2-NEMO code show good agreement with the one available in the literature. Furthermore, in the work, aerodynamic characteristics and aerothermodynamic environment of an entry capsule with hyperbolic contours were investigated by CFD analyses. Results show that the drag and lift coefficients, at the given freestream conditions, can be increased using hyperbolic contours when compared to the original forebody shape of the MSL entry vehicle. This implies that the ballistic coefficient can be reduced, while the reference area remains the same. From the work performed, it is evident that the hyperbolic contours can be utilized to design the shape of the forebody of the entry vehicles instead of the blunted nose cone. By considering the aerodynamic characteristics, aerothermodynamic environment, and the volume of the capsule, it is possible to design the optimum shape of the capsule with hyperbolic contours. Possible future work could include an analysis of the dynamic stability of the entry vehicles characterized by hyperbolic contours. Additionally, surface catalytic effects and turbulent models could be included once they become available in order to investigate their influence.

References

[1] Schoenenberger M. Dyakonov A. A. and Van Norman J. W. Hypersonic and Supersonic Static Aerodynamics of Mars Science Laboratory Entry Vehicle. *AIAA Paper 2012-2999*, 2012.

[2] Dyakonov A. A. Wright M. J. Tang C. Y. Edquist, K. T. Aerothermodynamic Design of the Mars Science Laboratory Heatshield. *41st AIAA Thermophysics Conference*, 2009.

[3] Hollis B. R. Dyakonov A. A. Laub B. Wright M. J. Rivellini T. P. Slimko E. M. Edquist, K. T. and W. H. Willcockson. Mars Science Laboratory Entry Capsule Aerothermodynamics and Thermal Protection System. *IEEEAC Paper 1423, IEEE Aerospace Conference, Big Sky, Montana*, 2007.

[4] H Otsu. Aerodynamic Characteristics of Re-Entry Capsules with Hyperbolic Contours. *Aerospace 2021, 8, 287. https://doi.org/ 10.3390/aerospace8100287.*

[5] Palacios F. Copeland S.R. Lukaczyk T.W. Alonso J.J. Economon, T.D. SU2: An Open-Source Suite for Multiphysics Simulation and Design. *AIAA J. 2016, 54, 828–846, doi:10.2514/1.J053813.*

[6] J.T. Garbacz C. Morgado F. Alonso J.J. Fossati M Maier, W.T. Needels. SU2-NEMO: An Open-Source Framework for High-Mach Nonequilibrium Multi-Species Flows. *Aerospace 2021, 8, 193. https://doi.org/10.3390/ aerospace8070193*, 2021.

[7] Duzel U. Hanquist K. M. Needels, J. T. and J. J. Alonso. Sensitivity Analysis of Gas-Surface Modeling in Nonequilibrium Flows. *AIAA Scitech 2022 Forum, 2022, p. 1636.*, 2022.

[8] Magin T.E. Scoggins, J.B. Development of Mutation++: Multicomponent Thermodynamic and Transport Properties for Ionized Plasmas written in C++. *In Proceedings of the 11th AIAA/ASME Joint Thermophysics and Heat Transfer Conference, Atlanta, GA, USA, 16–20 June 2014; p. 2966, doi:10.2514/6.2014-2966.*

[9] C Wilke. A viscosity equation for gas mixtures. *J. Chem. Phys. 1950, 18, 517–519.*

[10] M.; Ellis M. Blottner, F.G.; Johnson. Chemically Reacting Viscous Flow Program for Multi-Component Gas Mixtures. Technical report, Sandia Labs, Albuquerque, NM, USA, 1971.

[11] K.P. Thompson R.A. Yos J.M Gupta, R.N. Lee. A Review of Reaction Rates and Thermodynamic and Transport Properties for an 11-Species Air Model for Chemical and Thermal Nonequilibrium Calculations to 30,000 K. Technical report, NASA Langely Research Center, Hampton, VA, USA, 1990.

[12] A Eucken. Über das Wärmeleitvermögen, die spezifische Wärme und die innere Reibung der Gase. *Phys. Z 1913, 14, 324–332.*

[13] J.T. Garbacz C. Morgado F. Alonso J.J. Fossati M Tumuklu O. Hanquist K.M. Maier, W.T. Needels. Development of Physical and Numerical Nonequilibrium Modeling Capabilities within the SU2-NEMO Code. AIAA AVIATION 2023 Forum, 2023.

[14] SU2 Multiphysics Simulation and Design Software. SU2 User Guide, 2023. URL `https://su2code.github.io/docs_v7/home/`.

[15] D. S. Hollis B. R. Alter S. J. Loomis M. P. Edquist, K. T. Liechty. Aeroheating Environments for a Mars Smart Lander. *Journal of Spacecraft and Rockets, Vol. 43, No. 2, March-April, 2006, pp. 330-339.*

[16] J. T. Jaffe R. L. Candler G. V. Park, C. Howe. Review of Chemical-Kinetic Problems of Future NASA Missions, II: Mars Entries. *Journal of Thermophysics and Heat Transfer, Vol. 8, No.1, January-March 1994.*

[17] The MUlticomponent Thermodynamic and Transport library for IONized gases in C++. Github webpage, 2023. URL `https://github.com/mutationpp`.

[18] K.T. Edquist A.A. Dyakonov M.J. Wright C.Y. Tang. Aerothermodynamic environments definition for the Mars Science Laboratory entry capsule. , AIAA Pap. 1206 (2007) 8-11, 2007.

[19] G.V Neville, A.G.; Candler. Computational-Fluid-Dynamics-Based Axisymmetric Aeroshell Shape Optimization in Hypersonic Entry Conditions. *J. Spacecr. Rocket. 2015, 52, 76–88.*

[20] R.K Seager, C. Agarwal. Hypersonic Blunt-Body Shape Optimization for Reducing Drag and Heat Transfer. *J. Thermophys. Heat Transf. 2017, 31, 48–55.*

[21] R.D Theisinger, J.E. Braun. Multi-Objective Hypersonic Entry Aeroshell Shape Optimization. *J. Spacecr. Rocket. 2009, 46, 957–966.*

A. Appendix A

This appendix contains details of Mars's 8-species gas model, implemented in the Mutation++ thermochemical library by the author of the thesis. Thermochemistry models are implemented inside the Mutation++ library, which provides algorithms for the computation of thermodynamic, chemical kinetics, and transport gas properties. The selected 8-species Mars gas mixture model contains the following neutral species: CO_2, CO, N_2, O_2, NO, C, N, O. The reaction model utilized for the purpose of the analysis is the one proposed by Park [16]. Table 5 gives an overview of the implemented reaction model, where relevant neutral exchange and dissociation chemical reactions are presented with the corresponding reaction rate coefficients, given in the form:

$$k_r^f = CT_x^n exp(-T_d/T_x), \qquad (25)$$

where T_x is the temperature controlling the reaction and T_d is the characteristic temperature of the reaction. In the two-temperature environment of concern, T_x is taken to be T_a for dissociation reactions and T for the rest. T_a and T represent heavy particle translational-rotational temperature and geometric average temperature, respectively [16].

Reaction	M	C	n	T_d
$N_2 + M \rightarrow N + N + M$	C	3.0^{22}	-1.6	113200
	N	3.0^{22}		
	O	3.0^{22}		
	N_2	7.0^{22}		
	O_2	7.0^{21}		
	CO	7.0^{21}		
	NO	7.0^{21}		
	CO_2	7.0^{21}		
$O_2 + M \rightarrow O + O + M$	C	1.0^{22}	-1.5	59750
	N	1.0^{22}		
	O	1.0^{22}		
	N_2	2.0^{21}		
	O_2	2.0^{21}		
	CO	2.0^{21}		
	NO	2.0^{21}		
	CO_2	2.0^{21}		
$CO + M \rightarrow C + O + M$	C	3.4^{20}	-1	129000
	N	3.4^{20}		
	O	3.4^{20}		
	N_2	2.3^{20}		
	O_2	2.3^{20}		
	CO	2.3^{20}		
	NO	2.3^{20}		
	CO_2	2.3^{20}		
$NO + M \rightarrow N + O + M$	C	1.1^{17}	0	75500
	N	1.1^{17}		
	O	1.1^{17}		
	N_2	5^{15}		
	O_2	5^{15}		
	CO	5^{15}		
	NO	1.1^{17}		
	CO_2	1.1^{17}		
$CO_2 + M \rightarrow CO + O + M$	C	1.4^{22}	-1.5	63275
	N	1.4^{22}		
	O	1.4^{22}		
	N_2	1.4^{22}		
	O_2	6.9^{21}		
	CO	6.9^{21}		
	NO	6.9^{21}		
	CO_2	6.9^{21}		
$NO + O \rightarrow N + O2$		8.4^{12}	0	19450
$N_2 + O \rightarrow NO + N$		6.4^{17}	-1	38370
$CO + O \rightarrow C + O_2$		3.9^{13}	-0.18	69200
$CO_2 + O \rightarrow O_2 + CO$		2.1^{13}	0	27800

Table 5: Chemical reaction model for Martian atmosphere with reaction rate coefficients [16].

Abstract in lingua italiana

In tutte le precedenti missioni della NASA su Marte, la forma della parte anteriore della capsula che raggiunge la superficie del pianeta è stata progettata utilizzando un tronco di cono con apice sferico. Una forma alternativa della capsula può essere progettata utilizzando contorni iperbolici.

Questo lavoro indaga le caratteristiche aerodinamiche ipersoniche delle capsule di ingresso su Marte, progettate con contorni iperbolici, utilizzando il codice CFD SU2-NEMO. Viene anche analizzato l'ambiente aerotermodinamico in un punto della fase di rientro.

I risultati delle simulazioni CFD hanno dimostrato che i coefficienti di resistenza e di portanza possono essere aumentati utilizzando i contorni iperbolici, in confronto a quelli del veicolo di ingresso MSL original, senza alterare in modo significativo la forma della capsula. Ciò implica che le proprietà aerodinamiche del veicolo di ingresso possono essere migliorate utilizzando la forma del corpo anteriore basata sui contorni iperbolici.

Parole chiave: flusso ipersonico, veicoli di rientro su Marte, linee iperboliche della parte anteriore